

Excited States beyond Mott Gap in Half-Filled-Band Hubbard Model

Hisatoshi Yokoyama^{1*}, Kenji Kobayashi², Tsutomu Watanabe², and Masao Ogata³

¹*Department of Physics, Tohoku University, Aoba-ku, Sendai, 980-8578, Japan*

²*Department of Natural Science, Chiba Institute of Technology, Narashino, 275-0023, Japan*

³*Department of Physics and Trans-scale Quantum Science Institute, University of Tokyo, Bunkyo, Tokyo 113-0033, Japan*

In connection with recent experiments on excitation in which Mott insulators change to conductors, we study the properties of excited states beyond the Mott gap as quasi-stationary states for a two-dimensional Hubbard (t - t' - U) model at half filling. A variational Monte Carlo method is used with trial wave functions for paramagnetic or normal (PM), superconducting with $d_{x^2-y^2}$ -wave (d -SC), isotropic s -wave, and extended s -wave symmetries, and antiferromagnetic (AF) states. The excited states are generated by imposing a minimum number of doubly occupied sites (doublons) D_L on the lowest-energy states. For $U \gtrsim W$ (W : band width), $d_L = D_L/N_s$ (N_s : number of sites) corresponds to the excitation intensity. It is found that the AF state is the most stable among the states we treated for $d_L \lesssim 0.14$ and insulating. The PM and d -SC states become conductive over a threshold d_{Lc} , and the conduction is caused by unbound doublons and holons (empty sites). The PM state arises for $d_L \gtrsim 0.14$, but the d -SC state is always hidden by the AF state. The s -wave-type superconducting states are not stabilized for any parameter set.

1. Introduction

Recently, Mott-insulator-to-conductor transitions induced by ultrafast photoexcitation¹⁻⁴⁾ and pulse electric fields⁵⁾ with $\Delta E \gtrsim U$ (ΔE : excitation energy, U : onsite Coulomb repulsion or Mott gap) have been intensively studied with application to high-speed switching devices in mind. A similar experiment was also performed in cold-atom systems.⁶⁾ To date, related theoretical studies had shed light mostly on the dynamical aspects after such excitation.⁷⁻¹³⁾ The state after excitation develops or relaxes with ultra-high speeds, but it is also significant from a basic point of view to treat the states as quasi-stationary states, as previously studied using t - J -type models.¹⁴⁻¹⁶⁾ It is still nontrivial whether the “fresh” excited state (shortly after pumping) remains insulating or has changed to conductive.

In this study, we assume that the states excited beyond the Mott gap, in which extra doublons (doubly occupied sites, D) and holons (empty sites, H) are generated, are stationary for sufficiently long time for electronic processes. This assumption is not necessarily irrelevant, because relaxation processes through phonons and light emission can have much longer time scales. Here, we study these excited states as steady states using a two-dimensional Hubbard model at half filling by means of a variational Monte Carlo (VMC) method,¹⁷⁾ and reveal whether the stable excited state to be realized is insulating or conductive and what type of order prevails in it. In the VMC processes, small-scale energy ($E \ll U$) dissipates to the outside of the system, and it reaches the optimized state within the given condition of D mentioned below, in contrast with energy-conservative schemes.

As research in this line, various aspects of the states with fixed small numbers of doublons ($\mathcal{D} = 1 - 4$) were studied by applying an exact-diagonalization method to small clusters (~ 20 sites) of a t - J -type effective Hamiltonian without^{14,15)} and with¹⁶⁾ nearest-neighbor repulsive interaction. These pioneering studies showed important aspects of ex-

cited states, for instance, an antiferromagnetic (AF) order survives for weak excitation intensity, and repulsive correlation works between nearest-neighbor D-H pairs, as we will refer to. However, important problems have been left untouched. For instance, system-size dependence, which is crucial especially for $d_{x^2-y^2}$ -wave superconductivity,¹⁸⁾ is not easy to be checked. It is not clear how the effective Hamiltonian reproduces the properties of the original Hubbard model, for example, the effects of D and H already existing in the ground state were not clarified on the excited states. The properties of higher-energy states with $\Delta E \gtrsim U$, such as a $d_{x^2-y^2}$ -wave superconducting (d -SC) state, are still unknown. The present VMC scheme can shed light on these points.

To represent the excited states, we intentionally introduce additional doublons and holons into the trial states by prohibiting the total number of doublons (\mathcal{D}) from being smaller than the lower bound D_L we set ($\mathcal{D} \geq D_L$). This operation is exactly and easily carried out using the VMC method, and was found virtually equal to the creation of additional D_L doublons for $U \gtrsim U_c \sim W$ (U_c/t : the Mott transition point, W : band width). Thus, D_L and $D_L/N_s \equiv d_L$ (N_s : number of sites) corresponds to \mathcal{D} in the above studies for the t - J -type model and to the average intensity of photon absorption in the above photoexcitation experiments,²⁻⁴⁾ respectively. We apply this operation to a paramagnetic (PM) or normal state, an AF state, and superconducting (SC) states of three kinds of pairing symmetry, a $d_{x^2-y^2}$ wave, an isotropic s wave (s -SC) and an extended- s wave (x -SC), and study the properties of each state and mutual stability, in particular as functions of d_L [or equivalently of doublon density d in Eq. (14)].

It is intriguing to know whether the properties of the lowest-energy states^{17,18)} are preserved or change to different features in the excited states. For example, (i) all of the above states for $U > U_c$ or $U > U_{AF}$ (U_{AF}/t : AF transition point) are insulating in the lowest-energy cases. Are overabundant doublons and holons make the states conductive? (ii) the lowest-energy d -SC state exhibits robust pairing magnitude P_d im-

*yoko@cmpt.phys.tohoku.ac.jp

mediately below U_c/t (~ 6.6) and loses it in the Mott insulating regime ($U > U_c$). Does the excitation enhance (revive) or lower P_d (T_c)? (iii) Is the d -SC state, which is the most stable among the lowest-energy SC states, defeated by s -wave-type states, to which the η -pairing state¹³⁾ belongs, for $D_L > 0$?

This article is organized as follows: In Sect. 2, the model and method we use are introduced (Sect. 2.1), and the relation $D_L \sim \mathcal{D}$ for large U/t is confirmed (Sect. 2.2). In Sect. 3, we consider the excited states in the PM branch. In Sects. 4 and 5, the SC states and AF state are studied, respectively. In Sect. 6, we recapitulate the main results. In Appendix, we discuss the effects of diagonal hopping term. Preliminary results for d -SC state have been published in a proceedings.¹⁹⁾

2. Formalism

2.1 Model and Method

For addressing excited states with $\Delta E > U$, the single-band Hubbard model ($U \geq 0$) is suitable. We consider the case on a square lattice with diagonal transfer:

$$\begin{aligned} \mathcal{H} &= \mathcal{H}_{\text{kin}} + \mathcal{H}_U \\ &= - \sum_{(i,j),\sigma} t_{ij} (c_{i\sigma}^\dagger c_{j\sigma} + \text{H.c.}) + U \sum_j n_{j\uparrow} n_{j\downarrow}, \end{aligned} \quad (1)$$

where $n_{j\sigma} = c_{j\sigma}^\dagger c_{j\sigma}$ and (i, j) indicates the pairs on sites i and j . We set the hopping integral t_{ij} as t (≥ 0) for nearest neighbors, t' for diagonal (next-nearest) neighbors, and 0 otherwise ($\mathcal{H}_{\text{kin}} = \mathcal{H}_t + \mathcal{H}_{t'}$). As discussed in Appendix, t'/t dependence is undetectable in the AF state and not essential for the d -SC and PM states at least for $|t'/t| \lesssim 0.5$ and relevant excitation strength ($D_L/N_s \lesssim 0.08$). Hence, we fix t'/t at -0.3 (a typical value for cuprate superconductors) in the main text. We focus on the half-filled band ($n = N/N_s = 1$ or $\delta = |1 - n| = 0$, N : number of electrons). We use t and the lattice spacing as the units of energy and length, respectively.

To this model, we apply a variational Monte Carlo (VMC) method,^{17,20,21)} which enables us to exactly treat many-body wave functions and continuously connects weakly and strongly correlated regimes even if some phase transition lies between them. To construct trial excited states in which extra doublons and holons are induced, we extend the Jastrow form previously used for the lowest-energy state ($D_L = 0$) Ψ_0 ¹⁷⁾ to

$$\Psi_{D_L} (= \Psi_{d_L}) = \mathcal{P}_{D_L} \Psi_0, \quad (2)$$

where \mathcal{P}_{D_L} is a projector that imposes the condition $\mathcal{D} \geq D_L$.

Before explaining \mathcal{P}_{D_L} , we review $\Psi_0 (= \mathcal{P}\Phi = \mathcal{P}_G \mathcal{P}_Q \Phi)$. \mathcal{P}_G is the well-known Gutzwiller (onsite) projector:²²⁾

$$\mathcal{P}_G = \prod_j [1 - (1 - g)n_{j\uparrow}n_{j\downarrow}], \quad (3)$$

with a parameter g , \mathcal{P}_Q is a nearest-neighbor D-H binding factor^{18,23)} crucial for Mott physics: $\mathcal{P}_Q = \prod_j (1 - Q_j)$, where

$$Q_j = \zeta_d d_j \prod_\tau (1 - h_{j+\tau}) + \zeta_h h_j \prod_\tau (1 - d_{j+\tau}), \quad (4)$$

$d_j = n_{j\uparrow}n_{j\downarrow}$, $h_j = (1 - n_{j\uparrow})(1 - n_{j\downarrow})$, ζ_d and ζ_h are D-H binding parameters, and τ runs over all the nearest-neighbor sites of site j . At half filling, a relation $\zeta_d = \zeta_h$ ($\equiv \zeta$) holds owing to the electron-hole symmetry.

We turn to the one-body (determinantal) part Φ .²⁴⁾ As a PM

or normal state Φ_{PM} , we employ a Fermi sea

$$\Phi_{\text{PM}} = \prod_{\mathbf{k} \in \{\mathbf{k}\}_{\text{occ}}, \sigma} c_{\mathbf{k}\sigma}^\dagger |0\rangle, \quad (5)$$

where \mathbf{k} is inside the renormalized Fermi surface $\{\mathbf{k}\}_{\text{occ}}$; as explained below, four band parameters t_1 – t_4 are implicitly used to determine $\{\mathbf{k}\}_{\text{occ}}$. For the SC state, we use an N -electron BCS wave function with typical pairing-gap symmetries λ ($= d, s, \text{ or } x$),

$$\Phi_\lambda = \left(\sum_{\mathbf{k}} \phi_{\mathbf{k}} c_{\mathbf{k}\uparrow}^\dagger c_{-\mathbf{k}\downarrow}^\dagger \right)^{\frac{N}{2}} |0\rangle, \quad (6)$$

$$\phi_{\mathbf{k}} = \frac{v_{\mathbf{k}}}{u_{\mathbf{k}}} = \frac{\Delta_{\mathbf{k}}}{\varepsilon_{\mathbf{k}} - \mu + \sqrt{(\varepsilon_{\mathbf{k}} - \mu)^2 + \Delta_{\mathbf{k}}^2}}, \quad (7)$$

$$\Delta_{\mathbf{k}} = \begin{cases} \Delta_d(\cos k_x - \cos k_y) & d_{x^2-y^2}\text{-wave} \\ \Delta_s & \text{isotropic } s\text{-wave} \\ \Delta_x(\cos k_x + \cos k_y) & \text{extended } s\text{-wave} \end{cases}, \quad (8)$$

where Δ_d , Δ_s , and Δ_x represent pairing magnitude (not necessarily indicating coherence strength¹⁸⁾) of the respective symmetries, and are to be optimized. μ is a parameter, which is reduced to the chemical potential for $U/t \rightarrow 0$. For the AF state, a simple Hartree-Fock solution is used,

$$\Phi_{\text{AF}} = \prod_{\{\mathbf{k}\}_{\text{occ}}, \sigma} a_{\mathbf{k}\sigma}^\dagger |0\rangle, \quad (9)$$

$$a_{\mathbf{k},\sigma}^\dagger = \alpha_{\mathbf{k}} c_{\mathbf{k},\sigma}^\dagger + \text{sgn}(\sigma) \beta_{\mathbf{k}} c_{\mathbf{k}+\mathbf{Q},\sigma}^\dagger, \quad (10)$$

$$a_{\mathbf{k}+\mathbf{Q},\sigma}^\dagger = -\text{sgn}(\sigma) \beta_{\mathbf{k}} c_{\mathbf{k},\sigma}^\dagger + \alpha_{\mathbf{k}} c_{\mathbf{k}+\mathbf{Q},\sigma}^\dagger, \quad (11)$$

where \mathbf{Q} is the AF nesting vector (π, π) , $\text{sgn}(\sigma) = 1$ (-1) for $\sigma = \uparrow$ (\downarrow), and

$$\alpha_{\mathbf{k}} (\beta_{\mathbf{k}}) = \frac{1}{\sqrt{2}} \sqrt{1 - (+) \frac{\varepsilon_{\mathbf{k}}}{(\varepsilon_{\mathbf{k}})^2 + \Delta_{\text{AF}}^2}}. \quad (12)$$

Δ_{AF} corresponds to an AF gap parameter in the sense of the mean-field theory, but is renormalized owing to \mathcal{P} here.

In each Φ , a band renormalization effect (BRE) is introduced by optimizing the tight-binding band $\varepsilon_{\mathbf{k}}$, which is expanded up to sixth-neighbor sites:^{17,25)}

$$\varepsilon_{\mathbf{k}} = \gamma_{\mathbf{k}} + \varepsilon_1(\mathbf{k}) + \varepsilon_2(\mathbf{k}) + \varepsilon_3(\mathbf{k}) + \varepsilon_4(\mathbf{k}), \quad (13)$$

$$\gamma_{\mathbf{k}} = -2t(\cos k_x + \cos k_y), \quad (13a)$$

$$\varepsilon_1(\mathbf{k}) = -4t_1 \cos k_x \cos k_y, \quad (13b)$$

$$\varepsilon_2(\mathbf{k}) = -2t_2(\cos 2k_x + \cos 2k_y), \quad (13c)$$

$$\varepsilon_3(\mathbf{k}) = -4t_3(\cos 2k_x \cos k_y + \cos k_x \cos 2k_y), \quad (13d)$$

$$\varepsilon_4(\mathbf{k}) = -2t_4(\cos 3k_x + \cos 3k_y). \quad (13e)$$

Such BRE is crucial for considering PM and, especially, AF states.^{17,18)} The optimized band parameters t_1 – t_4 generally become different among Φ . Because the parameters in Φ (t_1 – t_4 , μ , Δ_d) have considerable redundancy, they are not optimized at unique values; however, the correlation parameters (g and ζ) as well as the minimal energy and corresponding physical quantities are uniquely determined within statistical errors.

It is known^{17,26–28)} that each Ψ_0 is (super)conducting for small U/t , brings about a first-order conductor-insulator tran-

Table I. Doubloon density d in lowest-energy states (Ψ_0 , $d_L = 0$) for relevant three phases in half-filled-band square lattice with $|t'/t| \leq 0.5$. For information, the data of a staggered flux (SF) phase²⁹⁾ are added. The data with * indicate that the optimized state is (super)conducting; the Mott²⁷⁾ (AF, PM-SF) transition point U_c/t ($\dagger U_{AF}/t$, $\# U_{SF}/t$) is shown in the last column. The values for $N_s = 14 \times 14$ are shown.

Ψ	d_0					U_c/t
	$U/t = 6$	8	10	12	20	
PM	*0.122	*0.055	0.019	0.015	0.007	~ 8.5
d -SC	*0.123	0.032	0.026	0.020	0.010	6.6
AF	0.083	0.055	0.038	0.027	0.011	$\dagger 3.0$
SF	0.109	0.031	0.023	0.017	0.009	$\# 5.0$

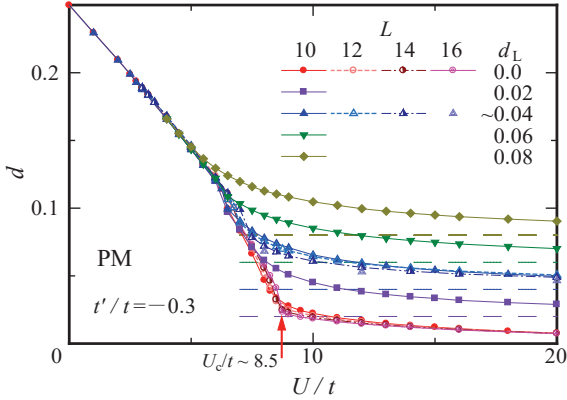


Fig. 1. (Color online) U/t dependence of doubloon density for some values of d_L and system size L estimated by VMC using Ψ_{PM} . Guide lines of $d = d_L$ are shown with long-dashed lines with the corresponding colors, to each of which d should converge for $U/t \rightarrow \infty$. The red arrow on the $d_L = 0$ curve indicates the Mott-transition point U_c/t .

sition at $U = U_c$ (Mott-transition point) for PM and SC states or at $U = U_{AF}$ (AF transition point) for AF state (see Table I), and becomes insulating for $U > U_c$ or U_{AF} . We take notice of excitation in the insulating regimes below, although we will also mention aspects near the transition points.

Now, we explain the projector \mathcal{P}_{D_L} in Eq. (2) for D-H excitations. It is known that the doubloon density,

$$d = \frac{D}{N_s} = \frac{1}{N_s} \sum_j \langle n_{j\uparrow} n_{j\downarrow} \rangle, \quad (14)$$

in the lowest-energy state Ψ_0 [denoted by ($d =$) d_0], is finite even in the insulating regime, as shown in Table I. In this regime, however, the doublons are tightly bound to the counter holons; therefore, there is no free charge carrier.³⁰⁾ As U/t increases, d decreases as $\propto t/U$ and completely vanishes in the limit of $U/t \rightarrow \infty$ (red curves in Fig. 1). By applying \mathcal{P}_{D_L} , we force Ψ_{D_L} to always have at least D_L doublons, where D_L is given in each calculation; in other words, \mathcal{P}_{D_L} restricts the space of Ψ_0 to $\mathcal{D} \geq D_L$, where \mathcal{D} indicates the number of doublons in an electron configuration. Therefore, $\Psi_{D_L=0}$ indicates the original Ψ_0 , and Ψ_{D_L} for $U/t = \infty$ is the state in which correctly D_L doublons (and holons) exist in any configuration: $\mathcal{D} = D_L$. For comparing different system sizes, it is convenient to use the lowest doubloon density $d_L \equiv D_L/N_s$ instead of the lowest number of doublons D_L . Similarly, we often write Ψ_{d_L} (\mathcal{P}_{d_L}) for Ψ_{D_L} (\mathcal{P}_{D_L}) in Eq. (2).

We compute expectation values with respect to Ψ_{d_L} using a VMC procedure similar to that used in Ref. 17. One can easily deal with \mathcal{P}_{d_L} in this procedure. We use systems of $N_s = L \times L$

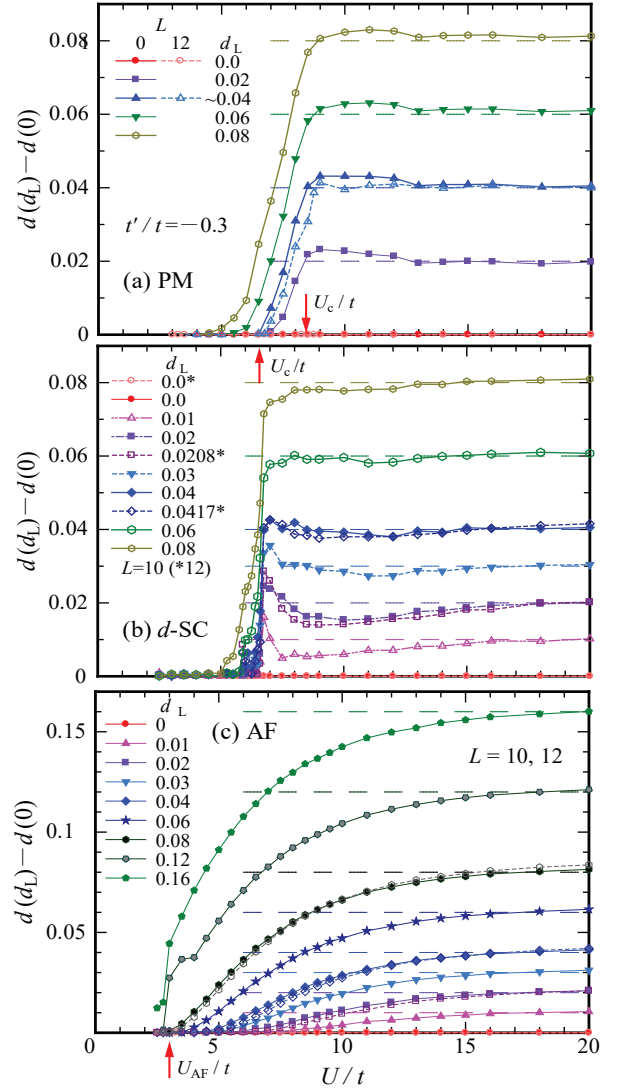


Fig. 2. (Color online) Increment of doubloon density [$\Delta d = d(d_L) - d(0)$] for various values of d_L as functions of U/t for (a) PM, (b) d -SC, and (c) AF states. The long-dashed lines in each panel indicates guide lines satisfying $\Delta d = d_L$ for respective d_L . In (c), similarly to (b), data for $L = 12$ are shown with open symbols and dashed lines for $d_L \sim 0.02, 0.04$, and 0.08 . The transition point in each state is indicated by a red arrow on a horizontal axis.

sites of $L = 10 - 16$ with the periodic-antiperiodic boundary conditions. In a sweep, we iterate processes of optimization typically 160 times for each parameter with 5×10^4 samples. We calculate the variational energy per site,

$$E = \frac{1}{N_s} \frac{\langle \Psi_{d_L} | \mathcal{H} | \Psi_{d_L} \rangle}{\langle \Psi_{d_L} | \Psi_{d_L} \rangle}, \quad (15)$$

with 2–40 (typically 6–10) different initial values (sweeps), because calculations are often trapped in metastable values near the global minimum,³¹⁾ and adopt the result with the lowest E and reasonable statistical errors as the optimized Ψ_{d_L} . Using this Ψ_{d_L} , we estimate expectation values of various quantities with 5×10^4 samples.

2.2 d_L as increment of doubloon density

In advance, we show by actual calculations that d_L approximately corresponds to the increment of d in excitations

(Δd). Figure 1 shows how U/t dependence of doublon density evolves as d_L is increased for the PM state. Let us write the doublon density for d_L as $d(d_L)$. In the case of $d \gg d_L$ in the metallic regime ($U < U_c$), $d(d_L)$ is almost independent of d_L , because Ψ_0 seldom includes configurations with $\mathcal{D} < D_L$. In the insulating regime ($U > U_c$), d seems to increase in proportion to d_L . To check this point, we show $\Delta d [\equiv d(d_L) - d(0)]$ in Fig. 2 when various values of d_L is imposed for the three states. For $\Psi_{d_L}^{(\text{PM})}$ and $\Psi_{d_L}^{(d\text{-SC})}$, the given d_L approximately leads to the increase in d (except for small d_L). For $\Psi_{d_L}^{(\text{AF})}$, $\Delta d(d_L)$ gradually approaches d_L as U/t increases, probably because the character of Ψ_{AF} as an insulator gradually varies from the Slater type to the Mott type. Anyway, we can consider that the relation $\Delta d = d_L$ is approximately realized in the Mott regime ($U > U_c \sim W$, W : band width) in the three states; as mentioned, Δd is proportional to the excitation intensity (e.g., optical intensity) in experiments.

3. Paramagnetic (Normal) States

Let us start with the behavior of the lowest-energy state Ψ_0 . In Fig. 1, a sign of the Mott transition is found as anomaly in d for $d_L = 0$ at $U_c/t \sim 8.5$ indicated by an arrow. Whether this indicates a Mott transition or not is confirmed by the behavior of momentum distribution function,

$$n(\mathbf{k}) = \frac{1}{2} \sum_{\sigma} \langle c_{\mathbf{k}\sigma}^{\dagger} c_{\mathbf{k}\sigma} \rangle, \quad (16)$$

and charge density structure factor,

$$N(\mathbf{q}) = \frac{1}{N_s} \sum_{i,j} e^{i\mathbf{q} \cdot (\mathbf{R}_i - \mathbf{R}_j)} \langle n_i n_j \rangle - n^2. \quad (17)$$

A previous study²⁷⁾ which treated Ψ_0 showed that a discontinuity at $\mathbf{k} = \mathbf{k}_F$ in $n(\mathbf{k})$, namely, Fermi surface (FS) disappears for $U > U_c$,³²⁾ and simultaneously $N(\mathbf{q})$ becomes quadratic-like for small $|\mathbf{q}|$,^{33,34)} as shown in Fig. 3 with small red stars for comparison, indicating that a gap opens in the charge sector.

Now, we consider how this Mott transition varies if extra doublons are created by introducing d_L . In Fig. 1, there is no anomaly found in d at $U \sim W$ for $d_L > 0$ even for large L (see for $d_L \sim 0.04$), suggesting that the Mott transition vanishes for $d_L > 0$. To corroborate it, in Fig. 3, $n(\mathbf{k})$ and $N(\mathbf{q})$ are shown for $d_L \sim 0.04$. In contrast to the case of $d_L = 0$ [see also Figs. 17 and 19 in Ref. 27], $n(\mathbf{k})$ exhibits discontinuities at near $(\pi, 0)$ and $(\pi/2, \pi/2)$ and the behavior of $N(\mathbf{q})$ for $|\mathbf{q}| \rightarrow 0$ is linear, both even for $U \gtrsim W$. Thus, the Mott transition vanishes at least for $d_L \sim 0.04$.

To consider the conductivity for $U > U_c$ in the PM and d -SC states, it is convenient to introduce a notion of ‘‘free doublon’’. In Mott insulators ($d_L = 0$ and $U > U_c$), almost all doublons are paired with holons (D-H bound pairs), and there is no free charge carrier (unpaired doublon or holon). This point is confirmed by the behavior of the D-H binding parameter ζ [Eq. (4)] shown in Fig. 4. For $d_L = 0$, ζ approaches 1 for $U > U_c$ as L increases, indicating that D-H pairs are tightly bound. However, as soon as d_L is introduced, ζ rapidly decreases and the D-H binding becomes weaker.³⁵⁾ Consequently, isolated doublons and holons will appear, which we call free doublons (holons). In the present wave function, a doublon without a holon(s) in the nearest-neighbor sites is

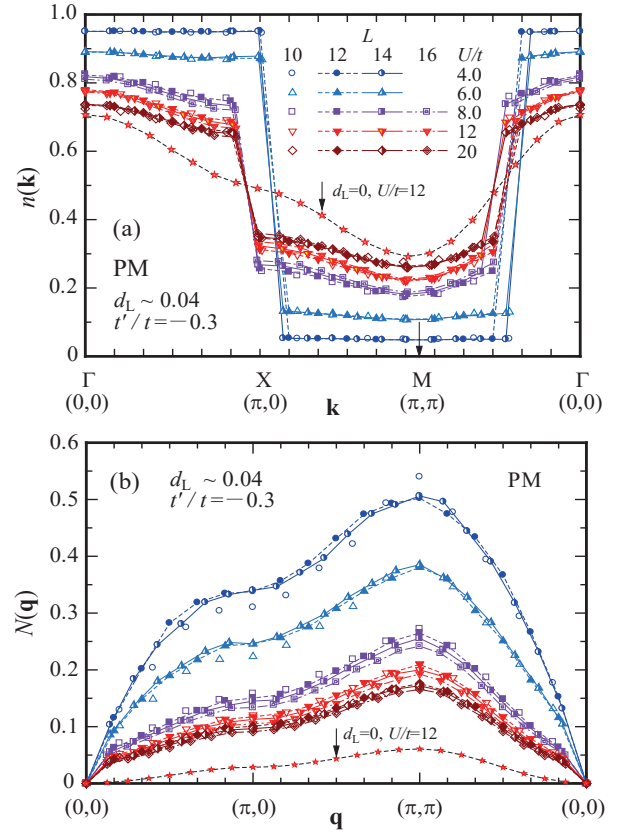


Fig. 3. (Color online) (a) Momentum distribution function and (b) charge-density structure factor in PM state with moderate value of $d_L \sim 0.04$ for several values of U/t and L along path of \mathbf{k} (\mathbf{q}): $(0,0) \rightarrow (\pi,0) \rightarrow (\pi,\pi) \rightarrow (0,0)$. For comparison, data for Ψ_0 ($d_L = 0$ and $U/t = 12$) are also plotted. Symbols and colors are common in the two panels.

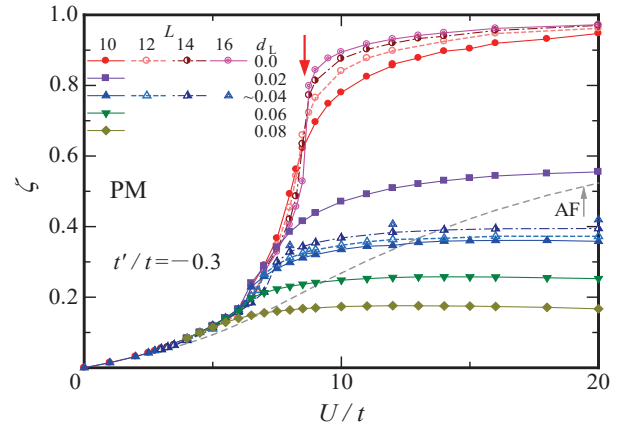


Fig. 4. (Color online) U/t dependence of optimized doublon-holon binding parameter in $\Psi_{d_L}^{(\text{PM})}$ for several values of excitation intensity d_L . The Mott transition point for $d_L = 0$ is indicated by a red arrow. For later comparison (in Sect. 5), the optimized ζ in the AF state for $d_L = 0$ and $L = 12$ is added with a gray dashed curve. As for d -SC, the behavior of ζ is essentially similar to the present case of $\Psi_{d_L}^{(\text{PM})}$.

regarded as a free doublon, because the present D-H binding factor \mathcal{P}_Q ranges over only the nearest-neighbor sites. Henceforth, the expectation value of the total number (density) of such free doublons is denoted by D_F ($d_F = D_F/N_s$). In Fig. 5(a), we show U/t dependence of d_F for various values of

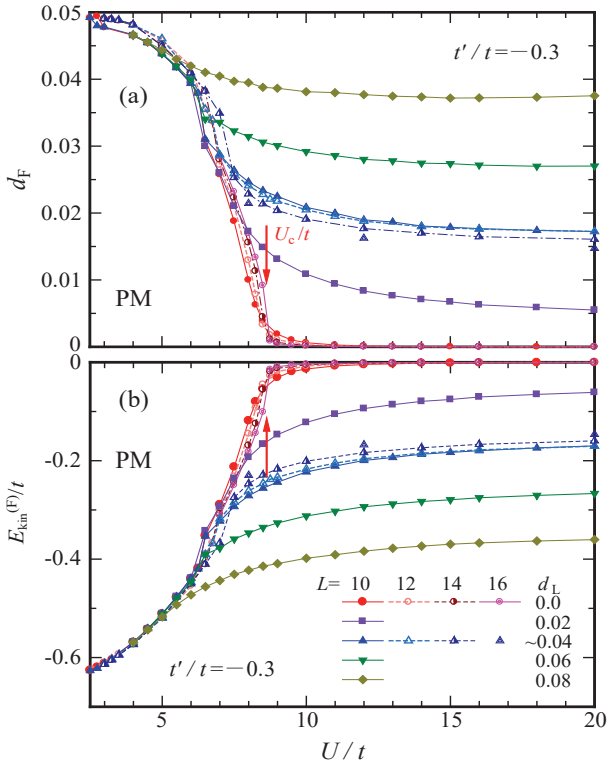


Fig. 5. (Color online) U/t dependence of (a) free doublon density and (b) part of kinetic energy $E_{\text{kin}}^{(F)}$, which stems from transfer of free doublons, for several values of d_L and L . The red arrows indicate the Mott transition point for $d_L = 0$. Symbols and colors are common in the two panels.

d_L . For $d_L = 0$, d_F becomes substantially zero for $U > U_c$.³⁶⁾ Namely, almost all doublons (recall Fig. 1 and Table I) exist as bound neutral D-H pairs. When d_L is raised to finite, free doublons come to survive for $U > U_c$, suggesting that these free doublons contribute to conductivity.

We can confirm this point by analyzing the kinetic energy $E_{\text{kin}} = \langle \mathcal{H}_{\text{kin}} \rangle$ into two contributions:

$$E_{\text{kin}} = E_{\text{kin}}^{(L)} + E_{\text{kin}}^{(F)}, \quad (18)$$

where $E_{\text{kin}}^{(L)}$ [$E_{\text{kin}}^{(F)}$] is the contribution from electron hopping that changes [preserves] \mathcal{D} .^{18,37)} $E_{\text{kin}}^{(L)}$ corresponds to the local process in which a D-H pair is created or destroyed and does not contribute to conductivity, whereas $E_{\text{kin}}^{(F)}$ chiefly consists of the global motion of free doublons or holons. In Fig. 5(b), $E_{\text{kin}}^{(F)}$ is shown as a function of U/t . One may notice that the behavior of $|E_{\text{kin}}^{(F)}|$ is quite similar to that of free-doublon density [Fig. 5(a)], indicating that free doublons and holons are the charge carriers.³⁸⁾

We next discuss how d_F behaves as a function of d_L or rather d for $U > U_c$; various quantities including d_F better scale to d than to d_L . The relation between d and d_L is shown for a typical value $U/t = 12$ in the inset of Fig. 6, and is broadly written as

$$d = d_L + d(0). \quad (19)$$

This relation is also read from Fig. 2 and available for the d -SC and AF states for large U/t . Thus, we often use d instead of d_L . In the main panel of Fig. 6, d dependence of d_F and $|E_{\text{kin}}^{(F)}|/t$ is shown. In weakly excited cases ($d \lesssim 0.1$, $d_L \lesssim 0.08$), d_F and $|E_{\text{kin}}^{(F)}|$ are proportional to each other. In strongly

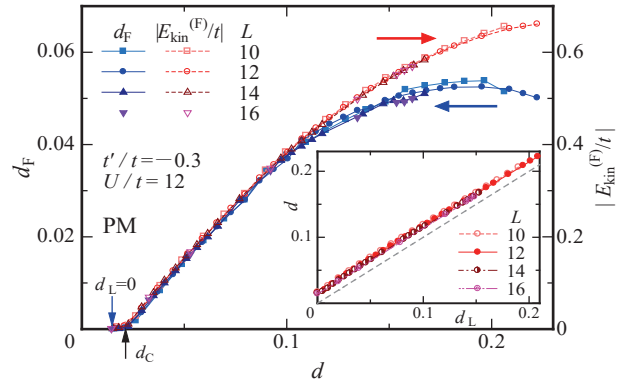


Fig. 6. (Color online) Free-doublon density (left axis) and its contribution to E_{kin}/t (right axis) as functions of doublon density. The blue arrow on the horizontal axis indicates the value of d in the lowest-energy state: $d(0)$. The black arrow indicates the threshold value of metallization d_c . The inset shows doublon density as a function of the given lowest doublon density. The gray dashed line shows a guide line of $d = d_L$.

excited cases ($d \gtrsim 0.1$, $d_L \gtrsim 0.08$), however, the behavior of $|E_{\text{kin}}^{(F)}|$ deviates from d_F , because hopping of a bound doublon between D-H pairs (clusters) comes to occur frequently as d increases and does not change d_F but contributes to $E_{\text{kin}}^{(F)}$.

In Fig. 6, we find a narrow but finite range of $d_F = 0$ for $d(0) < d < d_c \sim 0.02$ ($0 < d_L \lesssim 0.01$), where $\Psi_{d_L}^{(\text{PM})}$ is insulating. Therefore, we need finite excitation intensity d_c to metallize $\Psi_{d_L}^{(\text{PM})}$. This threshold d_c is somewhat larger for $\Psi_{d_L}^{(d\text{-SC})}$ as previously discussed [see Fig. 3(a) in Ref. 19]. The d -SC state remains insulating for $d_L \lesssim 0.022$.

4. Superconducting States

We first discuss the stability among the three SC states of different pairing symmetries. Previous studies for the lowest-energy state³⁹⁻⁴¹⁾ in strongly correlated regimes showed that the s -wave and extended s -wave SC states bring about no energy reduction, namely, the optimized $\Psi_0^{(s\text{-SC})}$ and $\Psi_0^{(x\text{-SC})}$ [Eq. (6)] are reduced to $\Psi_0^{(\text{PM})}$. On the other hand, $\Psi_0^{(d\text{-SC})}$ exhibits appreciable energy reduction for $U/t \gtrsim 5$.¹⁸⁾ These results are confirmed in Fig. 7(a), where the total energies for $d_L = 0$ are compared among the five states studied here as functions of U/t . As shown in Fig. 7(b), such situation does not qualitatively change in excited states of moderate d_L , although the energy gain owing to $\Psi_{d_L}^{(d\text{-SC})}$ appreciably decreases. Because we found no energy gain owing to $\Psi_{d_L}^{(s\text{-SC})}$ and $\Psi_{d_L}^{(x\text{-SC})}$ ($\Delta_s, \Delta_x = 0$) for any parameter set we studied, we will concentrate on the d -SC state in the following. We leave comparison with the AF state for Sect. 5.

A previous study^{26,27)} showed that the lowest-energy state $\Psi_0^{(d\text{-SC})}$ exhibits a Mott transition at $U = U_c \sim 6.6t$ [arrow in Fig. 7(a)]. Therefore, the excited states with extra doublons are meaningful for $U > U_c$, where $\Delta d \sim d_L$ as shown in Fig. 2(b). In this regime, various properties discussed for $\Psi_{d_L}^{(\text{PM})}$ in Sect. 3 applies to $\Psi_{d_L}^{(d\text{-SC})}$. The main point is that for $d_L > d_{Lc}$ [$d_{Lc} \sim 0.15$ (0.22) for $U/t = 8$ (12)], $\Psi_{d_L}^{(d\text{-SC})}$ becomes superconducting, whose charge carriers are free (unbound) doublons and holons ($d_F > 0$). Since this point was discussed in the preceding article,¹⁹⁾ here we consider what was not taken up there, especially, d (d_L) dependence.

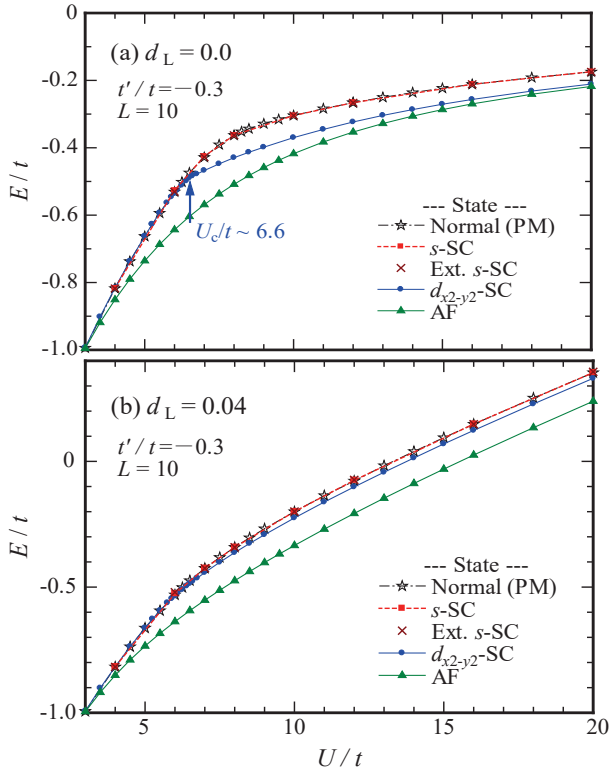


Fig. 7. (Color online) Comparison of total energy per site among states treated here as function of correlation strength for (a) lowest-energy state, and (b) moderate excited state ($d_L = 4$). In (a), the Mott-transition point of d -SC state is indicated by a blue arrow. For clarity, data only for $L = 10$ are plotted.

As a quantity to represent the strength of $d_{x^2-y^2}$ -wave SC, we use the d -wave nearest-neighbor pair correlation function $P_d(\mathbf{r})$ defined as,

$$P_d(\mathbf{r}) = \frac{1}{N_s} \sum_i \sum_{\tau, \tau' = \hat{x}, \hat{y}} (-1)^{1-\delta_{\tau, \tau'}} \langle \Delta_{\tau}^{\dagger}(\mathbf{R}_i) \Delta_{\tau'}(\mathbf{R}_i + \mathbf{r}) \rangle, \quad (20)$$

in which \hat{x} and \hat{y} denote the unit vectors in the x and y directions, respectively, and $\Delta_{\tau}^{\dagger}(\mathbf{R}_i)$ is the creation operator of a nearest-neighbor singlet,

$$\Delta_{\tau}^{\dagger}(\mathbf{R}_i) = (c_{i\tau}^{\dagger} c_{i+\tau\uparrow}^{\dagger} + c_{i+\tau\uparrow}^{\dagger} c_{i\downarrow}^{\dagger}) / \sqrt{2}. \quad (21)$$

Because $P_d(\mathbf{r})$ rapidly decays with $|\mathbf{r}|$ and has almost constant values for $|\mathbf{r}| \geq 3$ in the strongly correlated regimes (we actually checked it), we use, for accuracy, the average of $P_d(\mathbf{r})$ with $|\mathbf{r}| \geq 3$ as a typical value P_d .⁴²⁾ To measure the distance $|\mathbf{r}|$, we use so-called the Manhattan (stepwise) metric. For details of $P_d(\mathbf{r})$, see Ref. 18.

Figure 8(a) shows P_d as a function of U/t for various values of excitation intensity d_L . For $d_L = 0$, we know that P_d vanishes for $U > U_c$.²⁷⁾ For $0 < d_L < d_{Lc}$ ($0 < d < d_c \sim 0.037$),⁴³⁾ P_d is still substantially null for large U/t , as mentioned. In this range of d_L , $\Psi_{d_L}^{(d-SC)}$ remains insulating as shown in Fig. 9, in which $n(\mathbf{k})$ for $d_L \sim 0.01$ (light blue) has no discontinuity on the path of \mathbf{k} [even near $(\pi/2, \pi/2)$]. For $d_L > d_{Lc}$, P_d increases as d_L increases with a tail toward large U/t , becomes maximum at $d_L \sim 0.06$ ($d \sim 0.095$), and then decreases. This behavior of P_d becomes intelligible by plotting it as a function of d as shown in Fig. 8(b) for $U/t = 8, 12$ and 16 . The formation of d -SC order in this range of d_L is

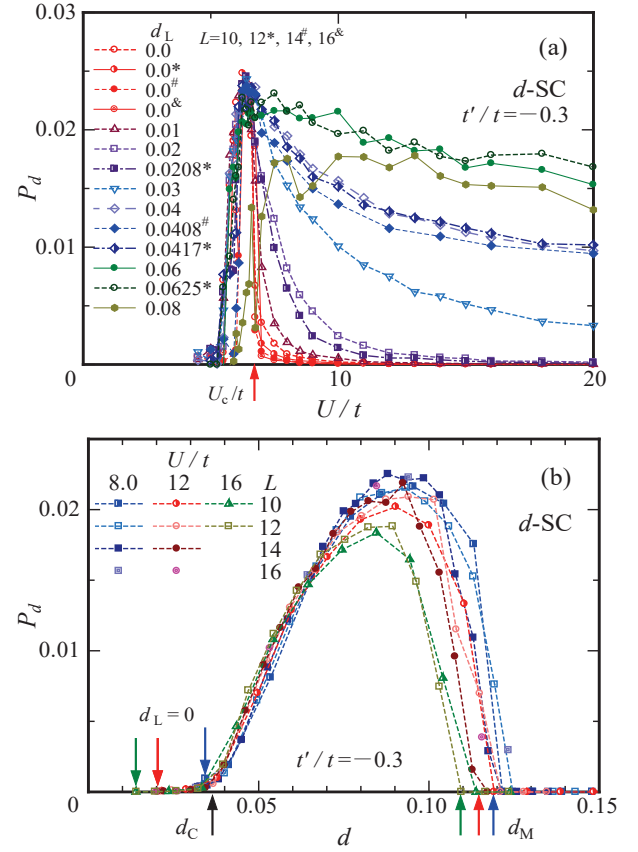


Fig. 8. (Color online) $d_{x^2-y^2}$ -wave SC correlation function as function of (a) interaction strength for various values of d_L and of (b) doublon density for $U/t = 8, 12$, and 16 . In (a), the Mott-transition point is indicated by a red arrow. In (b), some relevant values of d are indicated by arrows on the horizontal axis.

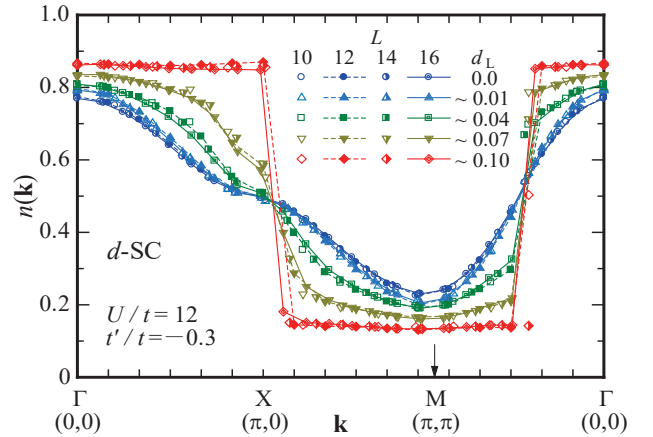


Fig. 9. (Color online) Momentum distribution function in d -SC state along same path as in Fig. 3(a) for various values of excitation intensity d_L for $U/t = 12$.

corroborated by the behavior of $n(\mathbf{k})$ in Fig. 9; for $d_L \sim 0.04$ and ~ 0.07 , $n(\mathbf{k})$ has no discontinuity near the antinodal point $\mathbf{k} = (\pi, 0)$ but exhibits a discontinuity (FS) near $(\pi/2, \pi/2)$ in the nodal direction.⁴⁴⁾ For $d \geq 0.1$, P_d rapidly drops and vanishes again at $d = d_M \sim 0.11-0.12$. $\Psi_{d_L}^{(d-SC)}$ becomes metallic for $d > d_M$, where $n(\mathbf{k})$ exhibits discontinuities both near $(\pi, 0)$ and $(\pi/2, \pi/2)$ as seen for $d_L \sim 0.10$ ($d \sim 0.12$) in Fig. 9.

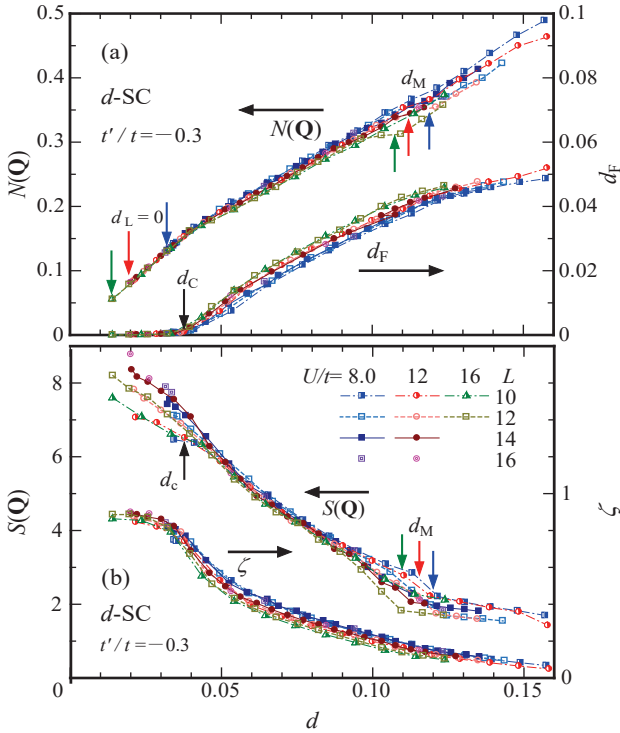


Fig. 10. (Color online) (a) Charge-density structure factor $N(\mathbf{q})$ at $\mathbf{q} = \mathbf{Q} = (\pi, \pi)$ and free doublon density, and (b) spin structure factor $S(\mathbf{Q})$ and optimized D-H binding parameter, as functions of doublon density for a few values of U/t . Symbols and lines are common in the two panels. The arrows of blue, red, and green for $d_L = 0$ and d_M indicate the data points of $U/t = 8, 12$, and 16 , respectively.

Thus, within $\Psi_{d_L}^{(d-SC)}$, a d -SC order forms for moderate excitation intensity $0.02 \lesssim d_L \lesssim 0.11$.

Note that the maximal value of P_d for a fixed value of U/t [Fig. 8(a)] is broadly equal to or slightly smaller than the corresponding value in chemically doped case [Fig. 24(b) in Ref. 18]. Furthermore, the maximum of P_d for $d_L > 0$ never becomes greater than that for $d_L = 0$ at $U \sim U_c$. These results suggest that higher T_c is not attained by D-H excitation at half filling, even if $\Psi_{d_L}^{(d-SC)}$ is realized.

Finally, we consider how charge and spin correlations evolves as excitation intensity is varied. In Fig. 10, we show d dependence of the charge-density structure factor $N(\mathbf{q})$ [Eq. (17)] and spin structure factor

$$S(\mathbf{q}) = \frac{1}{N_s} \sum_{ij} e^{i\mathbf{q} \cdot (\mathbf{R}_i - \mathbf{R}_j)} \langle S_i^z S_j^z \rangle, \quad (22)$$

at $\mathbf{q} = \mathbf{Q} = (\pi, \pi)$, where both $N(\mathbf{q})$ and $S(\mathbf{q})$ become maximum. The charge and spin correlations are scaled by doublon density rather than U/t . Generally, if repulsive electron correlation becomes stronger, $N(\mathbf{q})$ [$S(\mathbf{q})$] decreases [increases]. Therefore, Fig. 10 means that the D-H-pair excitation greatly weakens the effective electron correlation in the system; d_F increases and the D-H binding becomes loose (ζ decreases). Because the d -SC correlation in the present system is broadly given by the product of charge and spin correlations,^{18,45} The behavior of P_d is mainly controlled by $N(\mathbf{q})$ or d_F shown in Fig. 10(a) in the vicinity of d_c , but by the decay of AF spin correlation, which causes the d -SC pairing,⁴⁶ near d_M .

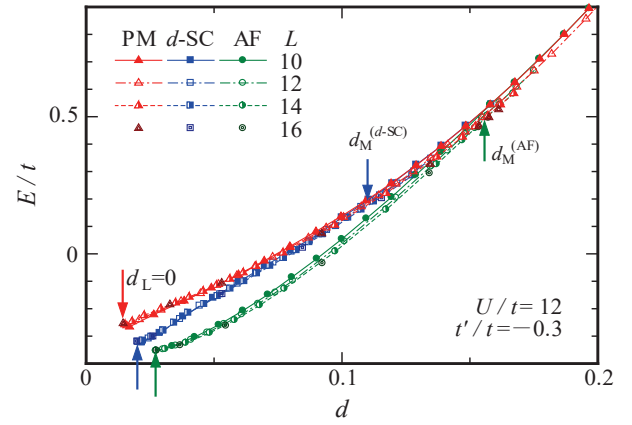


Fig. 11. (Color online) Comparison of total energy per site as functions of doublon density among Ψ_{PM} , Ψ_d , and Ψ_{AF} for $U/t = 12$. The boundary points d_M of the d -SC and AF orders are indicated by arrows. The situation is qualitatively the same for another $U/t (> U_c)$.

5. Antiferromagnetic States

To begin with, we study the stability of $\Psi_{d_L}^{(AF)}$. Figure 7(b) shows that the AF state has the lowest energy also in an excited state ($d_L = 0.04$) among the states treated here for $U > U_{AF}$. In Fig. 11, E/t is compared as functions of d for $U/t = 12$ [Eq. (19) is roughly valid here]; $\Psi_{d_L}^{(AF)}$ is still stable as long as m is finite ($d_L < d_{LM} \sim 0.14$). Thus, the AF state always overcomes the d -SC state in the d_L - U/t space, and will be realized as a stationary state. This aspect is consistent with the $\mathcal{D} = 1$ case (corresponding to $d_L = 0.0625$) of the previous study¹⁴) for the t - J -type model.

Therefore, it is important to study relevant properties of the AF state. The nature of AF gradually changes from a Slater type to a Mott type around $U = W = 8t$ in the lowest-energy state $\Psi_0^{(AF)}$.⁴⁷ This crossover seems to be preserved in the excited states as seen in Fig. 2(c), where Δd smoothly converges to the limiting values of $U/t \rightarrow \infty$. Thus, the present D-H excitation scheme is considered to be appropriate for $U \gtrsim W$ (Mott regime).

In Fig. 12(a), we show U/t dependence of the sublattice magnetization (an order parameter of AF),

$$m = \frac{2}{N_s} \sum_j \left| e^{i\mathbf{Q} \cdot \mathbf{r}_j} \langle S_j^z \rangle \right| \quad \text{with } \mathbf{Q} = (\pi, \pi), \quad (23)$$

which becomes 1 at the full moment. For $t'/t = -0.3$, the optimized state is paramagnetic for $U < U_{AF} \sim 3t$. At $U = U_{AF}$, $\Psi_{d_L}^{(AF)}$ exhibits a first-order AF transition and m discontinuously appears and gradually increases for $U > U_{AF}$. The transition value U_{AF}/t is almost independent of d_L , but becomes somewhat larger as d_L approaches the vanishing point $d_{LM} \sim 0.14$. In Fig. 12(b), d dependence of m is shown; as d (d_L) increases toward d_M (d_{LM}), m monotonically decreases and finally vanishes at a first-order transition point $d_M \sim 0.16$.

Now, we consider the conductivity of $\Psi_{d_L}^{(AF)}$ ($d_0 < d < d_M$) and $\Psi_{d_L}^{(PM)}$ ($d > d_M$). Figure 13 shows $n(\mathbf{k})$ and $N(\mathbf{q})$ of $\Psi_{d_L}^{(AF)}$ with $d_L \sim 0.04$ for four values of U/t . In contrast to the PM (Fig. 3) and d -SC [Figs. 4(b) and 5(b) in Ref. 19] states, which are always (super)conducting for $d \sim 0.04$, the AF is always insulating. Namely, $\Psi_{d_L}^{(AF)}$ exhibits no Fermi surface [discontinuity in $n(\mathbf{k})$] and is gapped [downward convex be-

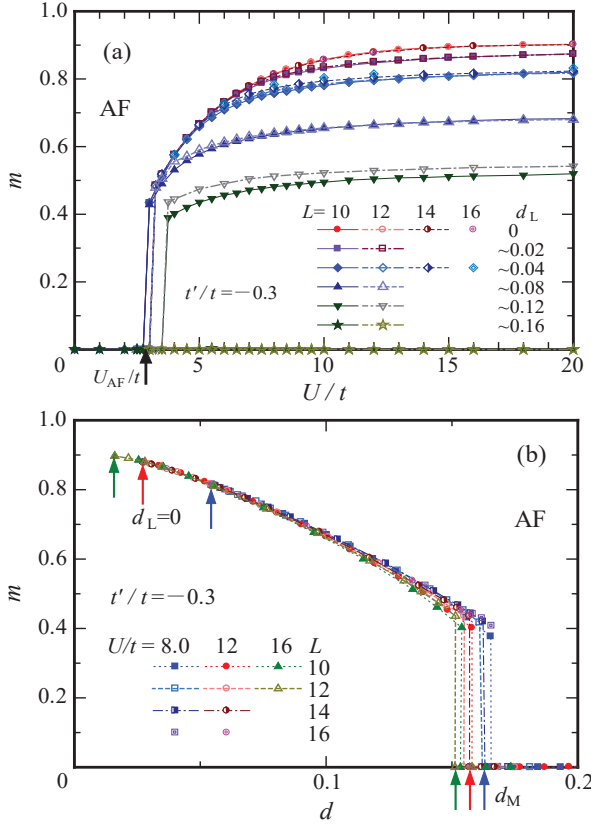


Fig. 12. (Color online) Sublattice magnetization of Ψ_{AF} , (a) as function of U/t for various values of excitation intensity d_L and L , and (b) as function of d for three values of U/t . The AF transition points (U_{AF}/t , d_M) are indicated respectively by arrows on the horizontal axes.

havior of $N(\mathbf{q})$ for $|\mathbf{q}| \rightarrow 0$]. In Fig. 14, we show the evolution of $n(\mathbf{k})$ as d_L increases for $U/t = 12$. As far as m is finite ($d_L < d_{LM} \sim 0.14$), the gap remains. A Fermi surface appears for $d_L > d_{LM}$. This behavior of the excited AF state (by introduction of D and H) is distinct from that of a partially filled AF state obtained by chemical doping with holons or doublons; the latter state is always metallic with pocket-type Fermi surfaces.¹⁸⁾ A fundamental difference between the two cases is whether the charge balance or neutrality is preserved (former) or not (latter) in the models.

In this connection, we mention the role of free doublons in $\Psi_{d_L}^{(AF)}$. As discussed in Sects. 3 and 4, free doublons and holons are responsible for conductivity in $\Psi_{d_L}^{(PM)}$ and $\Psi_{d_L}^{(d-SC)}$.

In Fig. 15, we plot d_F and $|E_{\text{kin}}^{(F)}|/t$ [in Eq. (18)] as functions of d . In contrast to the PM (Fig. 6) and d -SC [Fig. 10(a)] cases, free doublons and holons already exist in the lowest-energy state ($d_L = 0$) for $U/t = 8$ and 12, which is insulating. When doublons and holons are excited (as d_L or d increases), free-doublon density increases; d_F for $\Psi_{d_L}^{(AF)}$ is only somewhat smaller than d_F for $\Psi_{d_L}^{(PM)}$ and $\Psi_{d_L}^{(d-SC)}$. Nevertheless, the AF state is insulating as far as m is finite ($d < d_M$). This means that the D-H binding mechanism plays at most a subsidiary role for the insulation of the AF state. Actually, the optimized value of D-H binding parameter ζ for Ψ_{AF} is much smaller than those for the other states (Fig. 4). We should pursue the leading factor for the insulation of $\Psi_{d_L}^{(AF)}$.

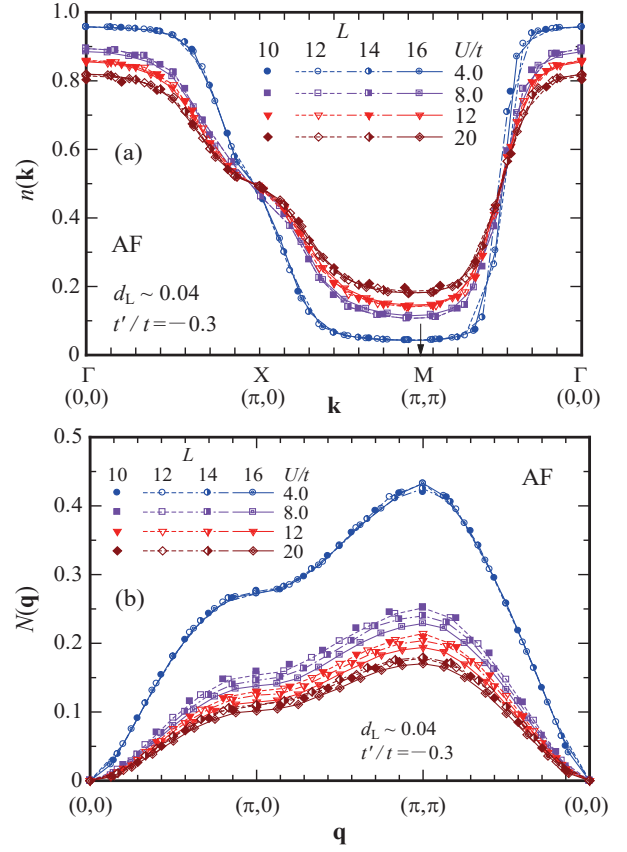


Fig. 13. (Color online) (a) Momentum distribution function and charge-density structure factor for AF state with $d_L \sim 0.04$ for four values of U/t and L along same path as in Fig. 3.

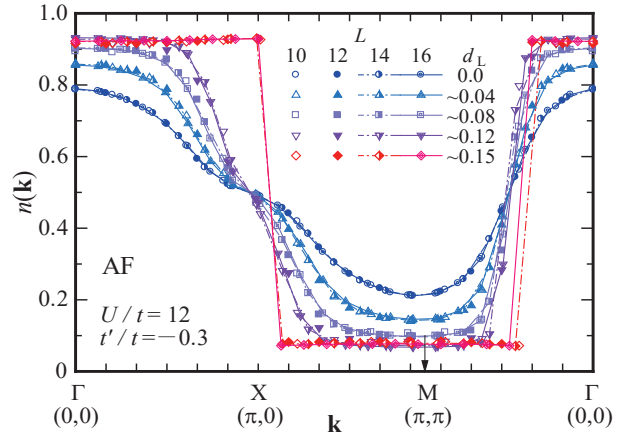


Fig. 14. (Color online) Momentum distribution function of Ψ_{AF} for $U/t = 12$. The excitation intensity d_L is varied.

6. Summary and Discussions

Assuming that high-energy quasi-stationary states are generated by photoexcitation or tera-Hertz pulse electric field, etc., we statically studied excited states exceeding the Mott gap ($\Delta E \geq U$) in the paramagnetic (normal), superconducting ($d_{x^2-y^2}$ -wave, s -wave, and extended s -wave symmetries), and antiferromagnetic branches for the Hubbard model at half filling. We applied a variational Monte Carlo method to the excited states by imposing the minimum doublon densities d_L

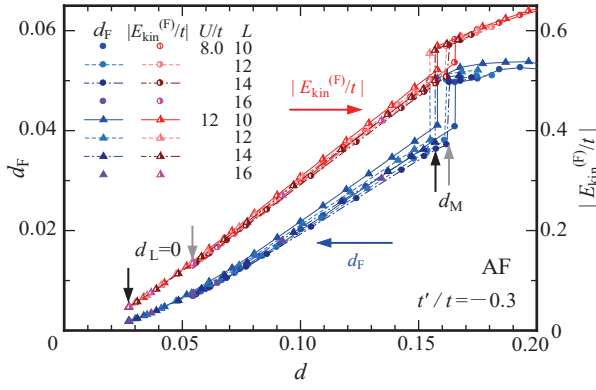


Fig. 15. (Color online) Free-doublon density (cool colors, left axis) and absolute value of $E_{\text{kin}}^{(F)}/t$ (warm colors, right axis) in AF state as functions of doublon density. The values of the lowest energy state ($d_L = 0$) and of transition points (d_M) are indicated by black ($U/t = 12$) and gray ($U/t = 8$) arrows.

on the trial states; d_L was found to correspond to the excitation intensity such as optical intensity per Cu site for cuprates. We recapitulate the main results including brief discussions in the following.

(1) In the PM and SC cases, the states become conductive over the threshold of excitation intensity d_{Lc} [~ 0.01 (PM), ~ 0.02 (d -SC)]. In this regime ($d_L > d_{Lc}$), free doublons and holons generated in excitation become charge carriers.

(2) In the same way as the lowest energy states, the SC states with s -wave and extended- s -wave symmetries have no energy gain over that of the PM state as excited states ($d_L > 0$) for any parameter set we checked. From this standpoint, an η -pairing state,⁴⁸⁾ which has an s -wave-type symmetry and may arise immediately after excitation,¹³⁾ is unlikely to be stable as a quasi-stationary state after some energy dissipation.

(3) The d -SC state becomes more stable than the PM state for intermediate excitation intensity $d_{Lc} \lesssim d_L \lesssim 0.11$; as a function of d_L , the pairing correlation function P_d exhibits a maximum at $d_L \sim 0.07$. The U/t dependence of P_d in $\Psi_{d_L}^{(d\text{-SC})}$ [Fig. 8(a)] is similar to the behavior of the chemically doped cases of the lowest-energy state $\Psi_0^{(d\text{-SC})}$ [Fig. 24(b) in Ref. 18]. The maximum of P_d is subtly smaller for $\Psi_{d_L}^{(d\text{-SC})}$ for any fixed value of U/t ($U > U_c$). Therefore, the strength of superconductivity (or T_c) induced by excitation at half filling is unlikely to exceed that obtained by doping holes to the lowest energy state (as usually done).

(4) The AF state is the most stable among the states we treated as far as the order parameter (m) is finite ($0 \leq d_L \lesssim 0.14$). Therefore, the AF state is reached after energy dissipation processes without changing the number of doublons. In contrast to the PM and d -SC states, the AF state preserves insulating in the whole excited regime of AF order. As a summary, we construct a semi-quantitative phase diagram in the U/t - d_L space shown in Fig. 16. There is no range where the d -SC order appears, which is always unstable toward the AF order. It follows that when experiments observe that the state is conductive,²⁻⁴⁾ the optical intensity is stronger than d_{LM} or the probes may observe the behavior of transient states.

(5) The effect of t' is qualitatively negligible for moderate d_L in all the states we addressed (see Appendix).

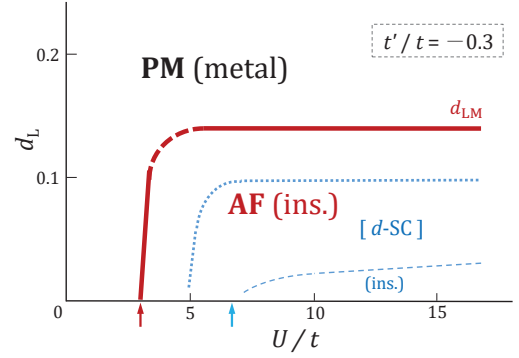


Fig. 16. (Color online) Semi-quantitative phase diagram of stationary D-H excited state in space of excitation intensity (d_L) and interaction strength (U/t) constructed within present wave functions. The loci of the conductor-insulator transitions for the two orders at $d_L = 0$ (U_{AF}/t , U_c/t) are indicated by arrows of corresponding colors, respectively. The d -SC state is always metastable and appears if the AF order is destroyed by some reason.

Finally, we add a comment on the relation between the present study with the previous ones¹⁴⁻¹⁶⁾ for a t - J -type model. In the present study, the bases of $\mathcal{D} < D_L$ are excluded, whereas the effects of $\mathcal{D} < \mathcal{D} - 1$ and $\mathcal{D} > \mathcal{D} + 1$ are not included in the previous studies. Therefore, the results may somewhat differ except for $U/t \rightarrow \infty$. In the last paper¹⁶⁾ of this series, effects of repulsive interaction between nearest-neighbor sites are considered, which turns to attractive interaction between nearest-neighbor D-H pairs. As a result, a phase separation takes place, where clusters of doublons and holons alternately sitting separate from domains of singly occupied sites. This phase-separated state is also insulating with partial AF orders. A conductive excited state may arise from another factor;⁴⁹⁾ we leave it for future studies.

Acknowledgment

One of the authors (HY) thanks Philipp Werner and the late Sumio Ishihara for comments on an early stage of this study. This work is supported in part by Grant-in-Aids from the Ministry of Education, Culture, Sports, Science and Technology, Japan.

Appendix: Effect of Diagonal Hopping

In previous papers,^{17,50)} we showed that the behavior of the lowest-energy states ($d_L = 0$) for $U > U_c$ at half filling becomes independent of t'/t at least for $|t'/t| \lesssim 0.5$ in various states (d -SC, AF, staggered-flux, and PM), if BRE is applied [see Fig. A-1(b) below for a d -SC case]. In this Appendix, we summarize the effects of the diagonal (next-nearest-neighbor) hopping term on the excited states ($d_L > 0$), and argue that t'/t does not affect the essence of this study for $|t'/t| \lesssim 0.5$.

Figure A-1 shows t'/t dependence of the total energy in the three states [(a) AF, (b) d -SC, and (c) PM] for a few values of d_L and L and $U/t = 12$.

(1) *AF state:* Like the $d_L = 0$ case, E/t (and the state) is unchanging at least for $|t'/t| \leq 0.8$ for small d_L ($\lesssim 0.04$). Even for relatively large d_L (~ 0.08), the optimized $\Psi_{d_L}^{\text{AF}}$ is unchanging for a wide range of t'/t ($|t'| < |\tilde{t}'|$, \tilde{t}' being the boundary value), and $|\tilde{t}'|/t$ increases as L increases, as indicated by arrows in Fig. A-1(a). In Fig. A-2(a), the staggered magnetization is shown; m remains finite even for $|t'| > |\tilde{t}'|$.⁵¹⁾

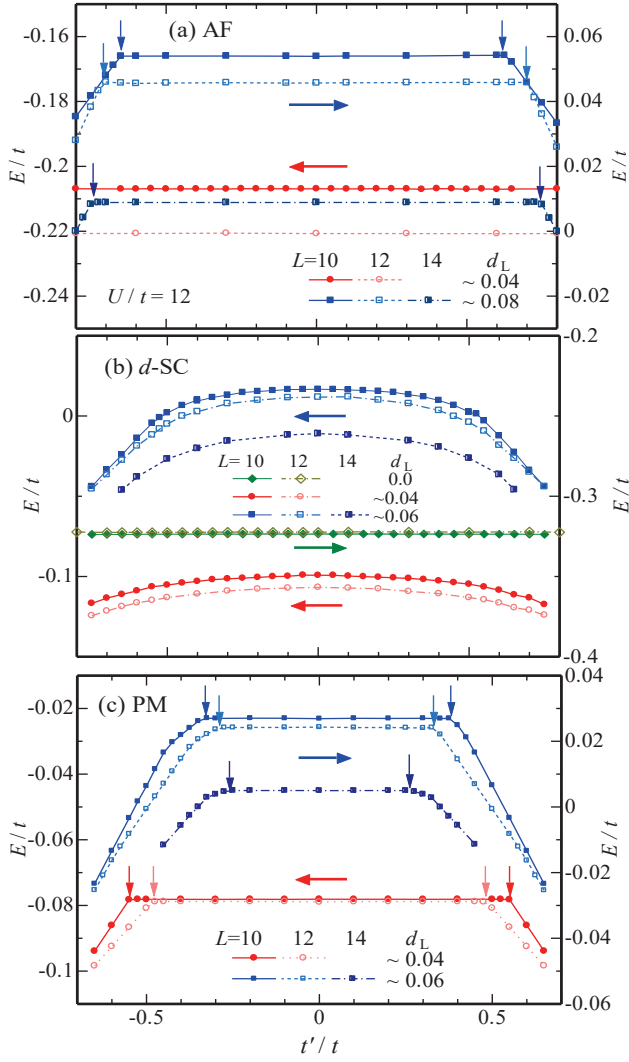


Fig. A.1. (Color online) Total energy as function of t'/t for some d_L and L ($U/t = 12$) in (a) AF, (b) d -SC, and (c) PM states. For $d_L = 0$ in (b), we cite previous data with BR2 (greenish symbols).¹⁷⁾ In (a) and (c), the boundaries \tilde{t}'/t are indicated by arrows with the color corresponding to each L . In every state for $d_L > 0$, E/t becomes subtly asymmetric with respect to $t'/t = 0$.

Thus, the AF state is robust against t'/t .

(2) d -SC state: E/t slowly changes as $|t'/t|$ increases for $d_L > 0$, in contrast to the AF state. For large d_L ($\gtrsim 0.06$), E/t comes to change rapidly for $|t'/t| \gtrsim 0.5$. In Fig. A-2(b), evolution of the d -SC correlation function P_d is shown. For $|t'/t| \lesssim 0.5$, P_d preserves large values regardless of d_L , whereas for $|t'/t| \gtrsim 0.5$, P_d rapidly drops for relatively large d_L . Especially for $t'/t \gtrsim 0.5$ (indicated by arrows), d -SC order vanishes and the state is reduced to the normal (PM) state.⁵²⁾

(3) PM state: Like the AF state, E/t (and the state) is unchanging for $|t'| < |\tilde{t}'|$ at least for finite L . However, $|\tilde{t}'|/t$ decreases as L increases. Therefore, for $L \rightarrow \infty$ (as the \mathbf{k} -point mesh becomes finer), E/t probably starts decreasing slowly as soon as t'/t is introduced like that of d -SC. Analyzing $n(\mathbf{k})$ (not shown), we found that t'/t dependence of Ψ_{PM} is almost limited to the loci of the Fermi surface. For $|t'| > |\tilde{t}'|$, the Fermi surface rapidly deviates from the antinodal points, and then $S(\mathbf{q})$ at $\mathbf{q} = \mathbf{Q}$ markedly decreases (not shown). This decrease of $S(\mathbf{Q})$ causes the rapid decrease of P_d for large $|t'/t|$ shown in Fig. A-2(b).

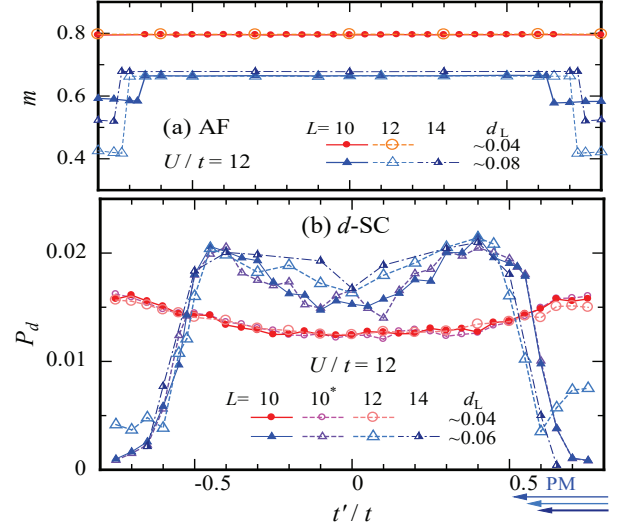


Fig. A.2. (Color online) Order parameters of (a) AF state m and (b) d -SC state P_d as functions of t'/t for some values of d_L and L . In (b), data for the two best trials are shown for $L = 10$ (as 10 and 10*) owing to large statistical errors. Judging from the vanishing of Δ_d , the d -SC state for $d_L \sim 0.06$ (bluish symbols) is reduced to the PM state for $t'/t \gtrsim 0.5$ as indicated by arrows of bluish colors (corresponding to different L with “PM”). In this area, P_d should vanish as $L \rightarrow \infty$.¹⁸⁾ On the other hand, weak d -SC order seems to remain for $t'/t \lesssim -0.5$.

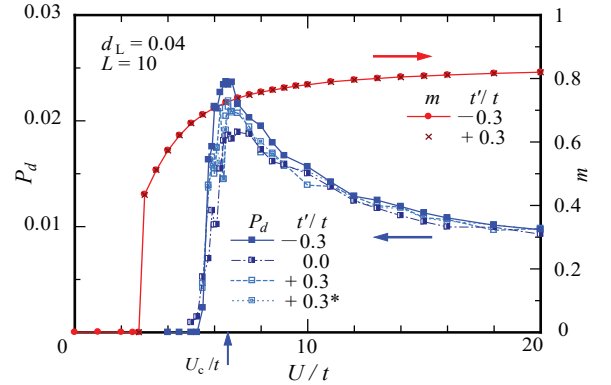


Fig. A.3. (Color online) U/t dependence of the order parameters m (right axis) and P_d (left axis) for $d_L = 0.04$ are respectively compared among a few values of $t'/t = \pm 0.3$. For P_d with $t'/t = +0.3$, which has relatively large errors, data of the two best trials of different initial conditions (indicated by +0.3 and +0.3*) are shown for each value of U/t . The Mott transition point of Ψ_d for $d_L = 0$ ($U_c/t \sim 6.6$) is indicated by an arrow on the horizontal axis.

Anyway, the order of energy ($E_{\text{PM}} \geq E_{d\text{-SC}} > E_{\text{AF}}$) is unchanging by introducing $|t'/t|$ ($\lesssim 0.8$). Finally, we mention U/t dependence. In Fig. A-3, the evolution, as U/t is varied, of the order parameters m and P_d for excited states ($d_L = 0.04$) is compared among a few values of t'/t . There is no detectable difference in m ($\lesssim 10^{-3}$) for any U/t , and P_d exhibits only a slight quantitative difference.

To summarize, t'/t dependence in the excited states is only quantitative for $|t'/t| \lesssim 0.5$; The properties for $t'/t = -0.3$ discussed in the main text are essentially unchanging for other moderate values of t'/t .

1) For instance, S. Iwai, M. Ono, A. Maeda, H. Matsuzaki, H. Kishida, H. Okamoto, and Y. Tokura, Phys. Rev. Lett. **91**, 057401 (2003).
2) H. Okamoto, T. Miyagoe, K. Kobayashi, H. Uemura, H. Nishioka,

- H. Matsuzaki, A. Sawa, and Y. Tokura, Phys. Rev. B **82**, 060513(R) (2010); Phys. Rev. B **83**, 125102 (2011).
- 3) T. Miyamoto, Y. Matsui, T. Terashige, T. Morimoto, N. Sono, H. Yada, S. Ishihara, Y. Watanabe, S. Adachi, T. Ito, K. Oka, A. Sawa, and H. Okamoto, Nat. Commun. **9**, 3948 (2018).
 - 4) T. Terashige, T. Ono, T. Miyamoto, T. Morimoto, H. Yamakawa, N. Kida, T. Ito, T. Sasagawa, T. Tohyama, and H. Okamoto, Sci. Adv. **5**, 2187 (2019).
 - 5) H. Yamakawa, T. Miyamoto, T. Morimoto, T. Terashige, H. Yada, N. Kida, M. Suda, H. M. Yamamoto, R. Kato, K. Miyagawa, K. Kanoda, and H. Okamoto, Nat. Mater. **16**, 1100 (2017).
 - 6) N. Strohmaier, D. Greif, R. Jördens, L. Tarruell, H. Moritz, T. Esslinger, R. Sensarma, D. Pekker, E. Altman, and E. Demler, Phys. Rev. Lett. **104**, 080401 (2010).
 - 7) For instance, H. Aoki, N. Tsuji, M. Eckstein, M. Kollar, T. Oka, and P. Werner, Rev. Mod. Phys. **86**, 779 (2014); S. Ishihara, J. Phys. Soc. Jpn. **88**, 072001 (2019).
 - 8) Z. Lenarčič and P. Prelovšek, Phys. Rev. Lett. **111**, 016401 (2013).
 - 9) E. Iyoda and S. Ishihara, Phys. Rev. B **89**, 125126 (2014).
 - 10) H. Yanagiya, Y. Tanaka, and K. Yonemitsu, J. Phys. Soc. Jpn. **84**, 094705 (2015).
 - 11) K. Shinjo and T. Tohyama, Phys. Rev. B **96**, 195141 (2017).
 - 12) P. Werner, J. Li, D. Golež, and M. Eckstein, Phys. Rev. B **100**, 155130 (2019).
 - 13) T. Kaneko, T. Shirakawa, S. Sorella, and S. Yunoki, Phys. Rev. Lett. **122**, 077002 (2019).
 - 14) A. Takahashi, S. Yoshikawa, and M. Aihara, Phys. Rev. B **65**, 085103 (2002).
 - 15) A. Takahashi, H. Gomi, and M. Aihara, Phys. Rev. B **66**, 115103 (2002).
 - 16) H. Gomi, A. Takahashi, T. Ueda, H. Itoh, and M. Aihara, Phys. Rev. B **71**, 045129 (2005).
 - 17) R. Sato and H. Yokoyama, J. Phys. Soc. Jpn. **85**, 074701 (2016).
 - 18) H. Yokoyama, M. Ogata, Y. Tanaka, K. Kobayashi, and H. Tsuchiura, J. Phys. Soc. Jpn. **82**, 014707 (2013).
 - 19) H. Yokoyama, K. Kobayashi, T. Watanabe, and M. Ogata, J. Phys.: Conf. Ser. **1590**, 012016 (2020).
 - 20) H. Yokoyama and H. Shiba, J. Phys. Soc. Jpn. **56**, 1490 (1987).
 - 21) C. J. Umrigar, K. G. Wilson, and J. W. Wilkins Phys. Rev. Lett. **60**, 1719 (1988).
 - 22) M. C. Gutzwiller, Phys. Rev. Lett. **10**, 159 (1963).
 - 23) H. Yokoyama and H. Shiba, J. Phys. Soc. Jpn. **59**, 3669 (1990).
 - 24) Although it is possible to use a mixed state of AF and SC orders, we leave such an integrated state for future studies.
 - 25) Because the optimized fifth-neighbor-site parameter t_5 in $\varepsilon_5(\mathbf{k}) = -4t_5 \cos 2k_x \cos 2k_y$ virtually becomes constant (zero), we do not include it in Eq.(13).
 - 26) H. Yokoyama, Y. Tanaka, M. Ogata, and H. Tsuchiura, J. Phys. Soc. Jpn. **73**, 1119 (2004).
 - 27) H. Yokoyama, M. Ogata, and Y. Tanaka, J. Phys. Soc. Jpn. **75**, 114706 (2006).
 - 28) As is known, dynamical-mean-field calculations led to analogous results on Mott transitions: A. Georges, G. Kotliar, W. Krauth, and M. J. Rozenberg, Rev. Mod. Phys. **68**, 13 (1996).
 - 29) H. Yokoyama, S. Tamura, and M. Ogata, J. Phys. Soc. Jpn. **85**, 124707 (2016).
 - 30) For instance, T. Miyagawa and H. Yokoyama, J. Phys. Soc. Jpn. **80**, 084705 (2011).
 - 31) It is not easy to perfectly remove the possibility of overlooking the true global minimum, although we carefully monitored every VMC sweep.
 - 32) In Ref. 27, in which BRE was not considered, the Mott transition point U_c/t shifts to large values as $|t'/t|$ ($t'/t < 0$) increases. If BRE is properly introduced, U_c/t becomes independent of $|t'/t|$ ($\lesssim 0.5$): $U_c/t \sim 8.5$.
 - 33) Within the single-mode approximation, $N(\mathbf{q})$ behaves for $|\mathbf{q}| \rightarrow 0$ as $\propto |\mathbf{q}|$ if the state is gapless in the charge sector, whereas $N(\mathbf{q}) \propto |\mathbf{q}|^\alpha$ ($\alpha \geq 2$) if a gap opens.³⁴⁾
 - 34) For instance, A. Auerbach, “Interacting Electrons and quantum Magnetism”, (Springer, New York, 1994).
 - 35) This tendency is consistent with that of the previous studies^{14,15)} for the t - J -type model, arguing that the D-H correlation between the nearest-neighbor sites is repulsive. In the present case, however, the D-H correlation remains attractive ($\zeta > 0$), because it is affected by the part of D and H already existing in the lowest-energy state ($d_L = 0$), which is strongly attractive as shown in Fig. 4 (red symbols).
 - 36) By considering the system-size dependence, d_F for $U > U_c$, which is finite for finite L , completely vanishes in the limit of $L \rightarrow \infty$.
 - 37) L. F. Tocchio, F. Becca, and C. Gros, Phys. Rev. B **83**, 195138 (2011).
 - 38) The reason why free doublons appear and increase as d_L increases is considered as follows. As d approaches d_L (for large U/t), it becomes difficult that the total energy is reduced by creating and, especially, destroying D-H pairs (namely, by $E_{\text{kin}}^{(L)}$), to keep the regulation $d \geq d_L$. To reduce the total energy, it becomes advantageous that D-H pairs are resolved and hopping of free doublons and holons arising thereby reduces $E_{\text{kin}}^{(F)}$.
 - 39) H. Yokoyama and H. Shiba, J. Phys. Soc. Jpn. **57**, 2482 (1988).
 - 40) C. Gros, Ann. Phys. (New York) **189**, 53 (1989).
 - 41) H. Yokoyama and M. Ogata, J. Phys. Soc. Jpn. **65**, 3615 (1996).
 - 42) It is known¹⁸⁾ that P_d measured using $\Psi_0^{(\text{PM})}$ (or $\Psi_0^{d-\text{SC}}$ with $\Delta_d = 0$) becomes finite for finite L but converges to zero for $L \rightarrow \infty$; actually, P_d looks almost vanishing for L as large as 30 (see Fig. C-1 in Ref. 18). Therefore, to avoid misunderstanding, we plot P_d as zero on purpose in the case where the optimized Δ_d becomes substantially zero, namely, Ψ_d is incoherent, in this article. Do not confuse it with a case of $P_d = 0$ with large Δ_d , as on the Mott-insulator side (small d_L for $U \gtrsim U_c$).
 - 43) Equation (19) is approximately valid in the d -SC case, but d_{LC} is somewhat dependent on U/t and L , in contrast with d_c . On the other hand, d_{LM} seems less dependent on U/t than d_M .
 - 44) A. Paramekanti, M. Randeria, and N. Trivedi, Phys. Rev. B **70**, 054504 (2004).
 - 45) F. C. Zhang, G. Gros, T. M. Rice, and H. Shiba, Supercond. Sci. Technol. **1**, 36 (1988).
 - 46) For instance, D. J. Scalapino, Phys. Rep. **250**, 330 (1995).
 - 47) For instance, S. Tamura and H. Yokoyama, J. Phys. Soc. Jpn. **84**, 064707 (2015).
 - 48) C. N. Yang, Phys. Rev. Lett. **63**, 2144 (1989).
 - 49) For example, band structure and intersite correlation. For the latter, see T. Ohgoe, M. Hirayama, T. Misawa, K. Ido, Y. Yamaji, and M. Imada, Phys. Rev. B **101**, 045124 (2020).
 - 50) T. Watanabe, H. Yokoyama, Y. Tanaka, and J. Inoue, J. Phys. Soc. Jpn. **75**, 074707 (2006).
 - 51) For $|t'| > |t|$, Ψ_{AF} becomes metallic with finite m . This state is similar to the carrier-doped AF state,¹⁷⁾ in which hole-pocket-type Fermi surfaces arise near $(\pi, 0)$ for $t'/t > 0$ and near $(\pi/2, \pi/2)$ for $t'/t < 0$. In the present case, because plus-charged (holons) and minus-charged (doublons) carriers are simultaneously generated, hole-pocket-type Fermi surfaces arise near $(\pi, 0)$ for $t'/t > 0$ [$(\pi/2, \pi/2)$ for $t'/t < 0$] and electron-pocket-type Fermi surfaces simultaneously arise near $(\pi/2, \pi/2)$ for $t'/t > 0$ [$(\pi, 0)$ for $t'/t < 0$].
 - 52) In this area ($t'/t \gtrsim 0.5$, $d_L \gtrsim 0.06$), we confirmed that Δ_d vanishes (not shown). For $t'/t \lesssim -0.5$, weak d -SC seems to remain ($\Delta_d > 0$).